Journal of Catalysis **195,** 12–19 (2000)
doi:10.1006/jcat.2000.2988, available online at http://www.idealibrary.com on IDEAL®

Infrared Spectroscopic Study of Acetonitrile on SnO_2-Based Thick Film and its Characteristics as a Gas Sensor

Jong Rack Sohn,*,[1] Hyo Derk Park,† and Duk Dong Lee‡

*Department of Industrial Chemistry, Engineering College, Kyungpook National University, Taegu 702-701, Korea; †Korea Electronics Technology Institute, Poungtaik 451-860, Kyoungki-do, Korea; and ‡Department of Electronic Engineering, Engineering College, Kyungpook National University, Taegu 702-701, Korea

Received September 17, 1999; revised June 26, 2000; accepted July 13, 2000

The $SnO_2/Al_2O_3/Pd$ and $SnO_2/Al_2O_3/Nb_2O_5/SiO_2$ thick film sensors were fabricated by screen printing and dipping methods, and their sensing characteristics to CH_3CN gas were investigated. The oxidation products of CH_3CN on the thick film were analyzed by FT-IR using a heatable gas cell. For the $SnO_2/Al_2O_3/Pd$ thick film, metallic Pd played a great role as a co-catalyst for the oxidation of CH_3CN. The IR results showed that the products formed by oxidation of CH_3CN at 300°C on the $SnO_2/Al_2O_3/Nb_2O_5$ thick film without SiO_2 were mainly CO_2, H_2O, and NH_3, while on the $SnO_2/Al_2O_3/Nb_2O_5/SiO_2$ thick film products such as CO_2, H_2O, N_2O, HNO_3, and HNO_2 were observed. The thick film devices containing SiO_2 showed high selectivity and negative sensitivity to CH_3CN due to the presence of nitrogen compounds produced by oxidation of CH_3CN. The optimum amount of Nb_2O_5 and operating temperature were 1.0 wt% and 300°C, respectively.

INTRODUCTION

Several commercial gas sensors make use of SnO_2 sensing elements. Gas sensors detecting a trace amount of the gases have applied to processes in the chemical, pharmaceutic, and fermentation industries to control the amount of the harmful wastes discharged from the plants, the explosion of the combustible gases and incomplete combustion, exhaust gases from automobiles, and testing in the clinics. The sensors show many advantages over optical or electrochemical sensors. The main advantages are their low cost, low consumption of electrical power, and high sensitivity.

The phenomenon of electrical conductivity changes induced in semiconducting materials by adsorption of gases on the solid surface is increasingly being used as a means of flammable and toxic gas detection. The working mechanism of thick film and sintered gas sensors is based on the buildup of Schottky barriers between adjacent grains caused by the ionosorbed oxygen (1).

Semiconductor gas sensors using SnO_2 and ZnO have been studied extensively since they were proposed by Seiyama *et al.* (2). Successively, several research laboratories worked with the aim of developing new devices. The recent research on flammable gas sensors has concentrated on SnO_2 in the form of thick film and sintered ceramics (3–5).

However, sensors should be improved due to a lack of stability and a poor selectivity. The addition of small amounts of additives is known to provide better sensitivity and selectivity (6, 7). An improvement of the selectivity of sensors besed on SnO_2 is generally obtained by adding some specific catalysts such as Pd or Pt for heavy combustible gases (8–10), CeO_2 for hydrogen (11), and ThO_2 for CO (12).

In this work, we have developed a SnO_2-based sensor for the detection of acetonitrile gas, which is known to be a poisonous chemical at low levels in air. The sensing characteristics of a SnO_2-based sensor to acetonitrile were studied by FT-IR analyses of gaseous species produced by oxidation of CH_3CN on the sensor surface.

EXPERIMENTAL

Al_2O_3 (10.0 wt%) and Nb_2O_5 (0.2–2.0 wt%) [or $PdCl_2$ (0–5.0 wt%)] were mechanically mixed with the base material, SnO_2, followed by calcination in air at 600°C for 1 h. Al_2O_3, Nb_2O_5, SnO_2, and $PdCl_2$ were obtained from Aldrich, Milwaukee, WI, where the purity of the samples was 99.9%. Al_2O_3 was used to improve the stability of the fabricated sensor and to give a strong cohesion between the thick film and alumina substrate. The calcined sample was ground and then mixed with water to prepare a paste. The paste was screen-printed onto an alumina substrate and then dipped into tetraethylorthosilicate solution followed by sintering in air at 700°C for 1 h. Figure 1 shows the fabrication process of the thick film sensor. The sensor sensitivity was measured in a stainless steel box equipped with a heater, as described in a preceding publication (13).

The sensitivity is defined as R_g/R_0, where R_0 and R_g are the electric resistances in fresh air and in the test gas, respectively. The products formed by the oxidation reaction of

[1] To whom correspondence should be addressed.

0021-9517/00 $35.00

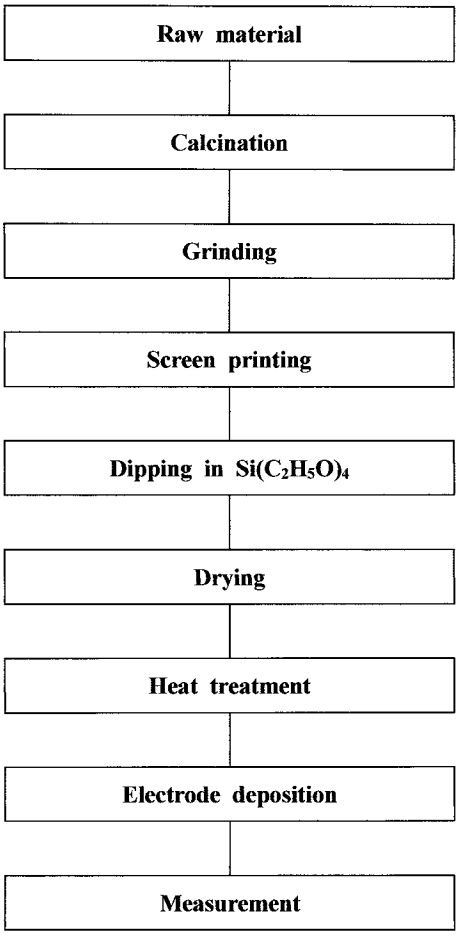

FIG. 1. Fabrication flow chart of a thick film sensor.

CH_3CN on the sensor surface were analyzed by a Mattson Model GL 6030E FT-IR spectrometer using a heatable IR gas cell. FT-IR absorption spectra were measured over the range of 4000–400 cm^{-1}.

X-ray photoelectron spectra were obtained with a VG Scientific model ESCALAB MK-11 spectrometer. Al $K\alpha$ and Mg $K\alpha$ were used as the excitation source, usually at 12 kV, 20 mA. The analysis chamber was at 10^{-9} Torr or better, and the spectra of the sample, as fine powder, were analyzed. Binding energies were referenced to the C_{1s} level of the carbon at 284.6 eV.

X-ray diffraction patterns of samples were obtained by means of a JEOL model JDX-8030 diffractometer, employing Cu $K\alpha$ (Ni-filtered) radiation. The specific surface area was determined by applying the BET method to the adsorption of N_2 at −196°C.

RESULTS AND DISCUSSION

The optimum base material was selected based on the decomposition temperature of CH_3CN on the surface of various metal oxides and on the FT-IR analyses of the decomposed products. The decomposition temperature of CH_3CN is defined as the temperature at which the decomposed products are observed in the IR spectra after the reaction for 0.5 h. The decomposition reaction was carried out in a heatable gas IR cell under the condition of 20 Torr CH_3CN and 500 Torr air, where 16–20 Torr CH_3CN was the most appropriate to observe the IR spectra in a gas cell. The decomposition temperature of CH_3CN on metal oxides and their surface areas are listed in Table 1. On the surface of SnO_2, CH_3CN began to decompose at 130°C and many

TABLE 1

Decomposition Temperature of CH_3CN on Metal Oxides and Their Specific Surface Area

Metal oxide	Type	Decomposition temperature (°C)	Surface area (m^2/g)
SnO_2	n	130	5.0
WO_3	n	150	4.4
CoO	p	200–220	4.5
TiO_2	n	230	6.1
Fe_2O_3	n	250	3.0
ZnO	n	>300	4.8

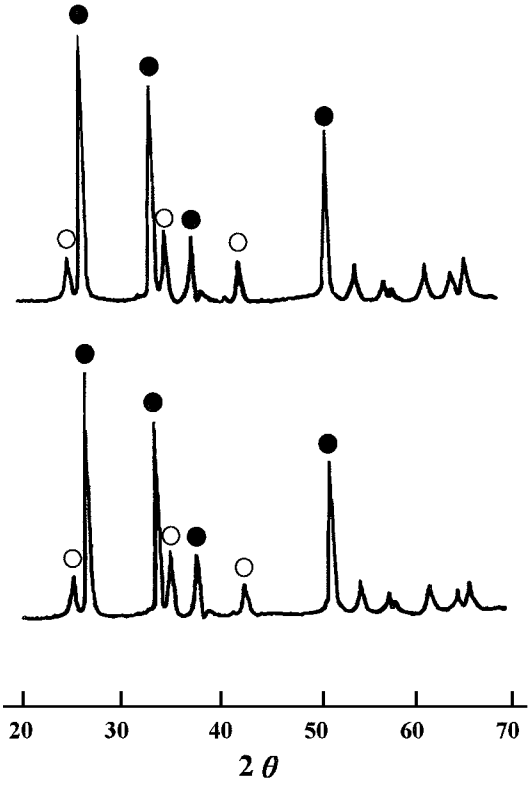

FIG. 2. X-ray diffraction patterns of $SnO_2/Al_2O_3/Nb_2O_5$ and $SnO_2/Al_2O_3/Nb_2O_5/SiO_2$ calcined at 700°C for 1 h: ●, tetragonal phase of SnO_2; ○, α-Al_2O_3 phase.

products were produced at 300°C. The products from the decomposition reaction were H_2O, NH_3, CO_2, and N_2O. The easiness of decomposition on the surfaces of metal oxides falls in the following sequence:

$$SnO_2 > WO_3 > CoO > TiO_2 > Fe_2O_3 > ZnO.$$

The crystalline structures of $SnO_2/Al_2O_3/Nb_2O_5$ and $SnO_2/Al_2O_3/N_2O_5/SiO_2$ sintered in air at 700°C for 1 h were examined. As shown in Fig. 2, for both samples only the tetragonal phase of SnO_2 and α-Al_2O_3 phase were observed. The crystalline phases of Nb_2O_5 and SiO_2 did not appear, indicating that they are amorphous or the crystallites formed are less than 4 nm in size, that is, beyond the detection capability of the XRD technique (14).

Figure 3 shows the IR spectra of CH_3CN (16 Torr) and the oxidation products of CH_3CN on SnO_2 and CoO thick films under the condition of 16 Torr CH_3CN and 16 Torr air at 300°C for 0.5 h. For pure CH_3CN, the bands at 2967 and 2940 cm^{-1} are assigned to the CH_3 stretching vibration mode, while those at 1444 and 1381 cm^{-1} are ascribed to the CH_3 deformation (15). The bands at 2299 and 2260 cm^{-1} are assigned to the CN stretching vibration. However, on the SnO_2, the bands due to NH_3 and CO_2 in addition to CH_3CN were observed as shown in Fig. 3. The bands at 3414, 1624, 964, and 930 cm^{-1} are ascribed to the NH_3, while those at 3723, 3635, 2361, and 667 cm^{-1} are due to the CO_2 (16). Oxidation of CH_3CN on SnO_2 seems to proceed by the following reaction:

$$CH_3CN + 2O_2 = NH_3 + 2CO_2. \quad [1]$$

On CoO, the bands due to CO_2 were observed similarly to the case of SnO_2, but the bands due to NH_3 did not appear. Instead of NH_3 bands, those due to N_2O and H_2O were observed. The bands at 2238 and 2211 cm^{-1} (doublet) and 1300 and 1273 cm^{-1} (doublet) are ascribed to the N_2O (16), while those at 3459 and 1624 cm^{-1} are due to the H_2O. N_2O and H_2O seem to form by the oxidation of NH_3 produced

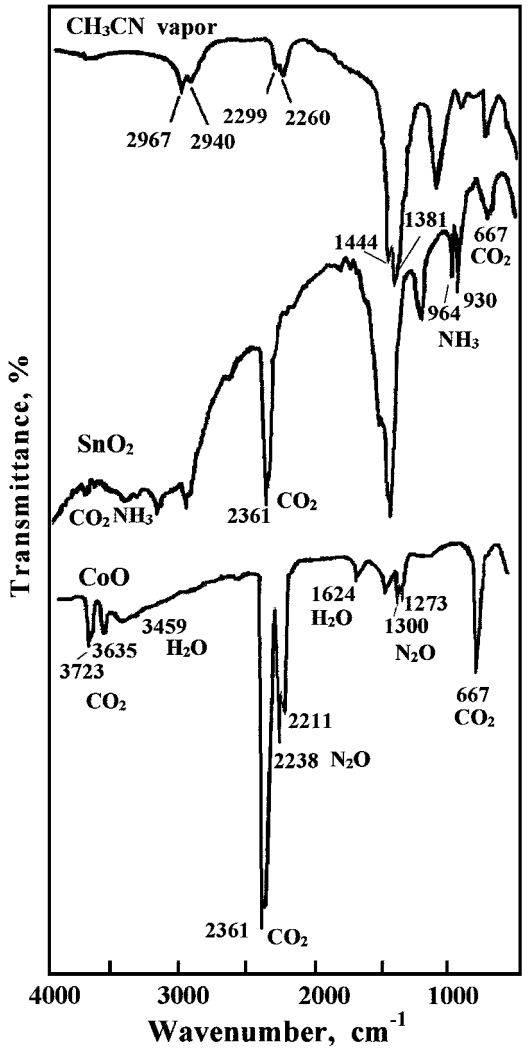

FIG. 3. Infrared spectra of CH_3CN and the oxidation reaction products of CH_3CN on SnO_2 and CoO thick films.

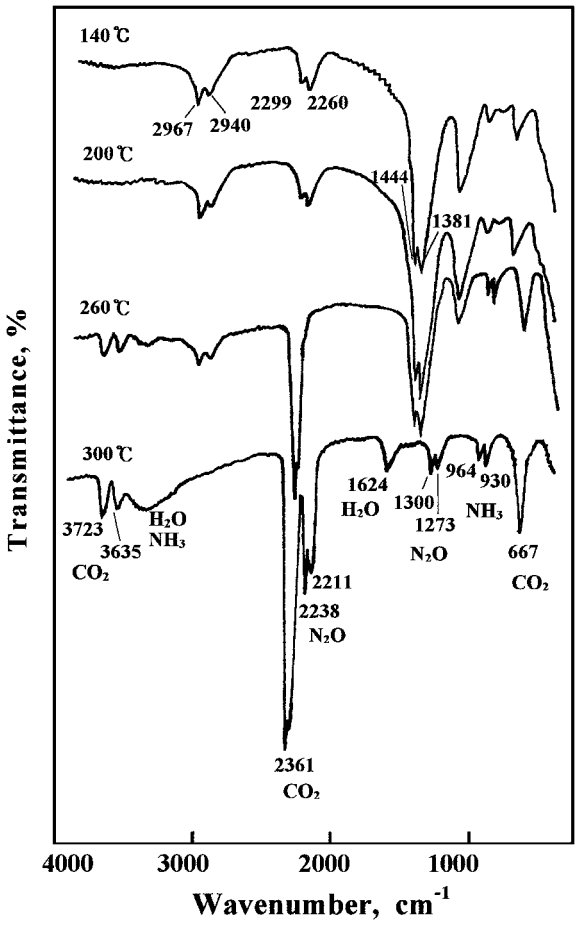

FIG. 4. Infrared spectra after an oxidation reaction of CH_3CN on SnO_2/Al_2O_3/Pd (0.2 wt%) at various temperatures.

by Eq. (1) as follows:

$$2NH_3 + 2O_2 = N_2O + 3H_2O. \quad [2]$$

Figure 4 shows infrared spectra of gases produced by oxidation of CH_3CN on SnO_2/Al_2O_3/Pd (0.2 wt%) at various temperatures for 20 min, where the concentrations of CH_3CN and air are 20 and 300 Torr, respectively. In the range of 140–200°C, no bands except for CH_3CN were observed, indicating that the oxidation of CH_3CN did not occur. However, at 240°C, bands due to CO_2 (2361 cm^{-1}) and NH_3 (964 and 930 cm^{-1}), appeared, indicating that the oxidation reaction occurred according to Eq. [1]. At 300°C, as shown in Fig. 4, most of the CH_3CN was oxidized and the bands due to N_2O (2238 and 2211 cm^{-1}) and H_2O (1624 cm^{-1}) appeared as a result of the oxidation of NH_3 produced by Eq. [1] according to Eq. [2].

It is well known that Pd is a very active catalyst for a variety of oxidation reactions (17, 18). The oxidation state of Pd in a SnO_2/Al_2O_3/Pd thick film sintered at 700°C for 1 h was examined by XPS of Pd 3*d*. As shown in Fig. 5, the oxidation states of Pd were 4+, 2+, and 0 with the relative ratio of 56 : 29 : 15. The major oxidation state of Pd was 2+ with a relative content of 56% and the existence of metallic Pd was confirmed as shown in Fig. 5. Yamazoe and co-workers also proved the presence of metallic Pd particles in their SnO_2 sintered at 600°C by X-ray diffraction analyses (19). $PdCl_2$ seems to decompose into metallic Pd, which is mainly oxidized to PdO in air below 650°C. At higher temperature, PdO seems to undergo further oxidation to PdO_2. In the case of SnO_2/Al_2O_3/Pd it seems likely that metallic Pd plays a significant role as a co-catalyst for the oxidation of CH_3CN.

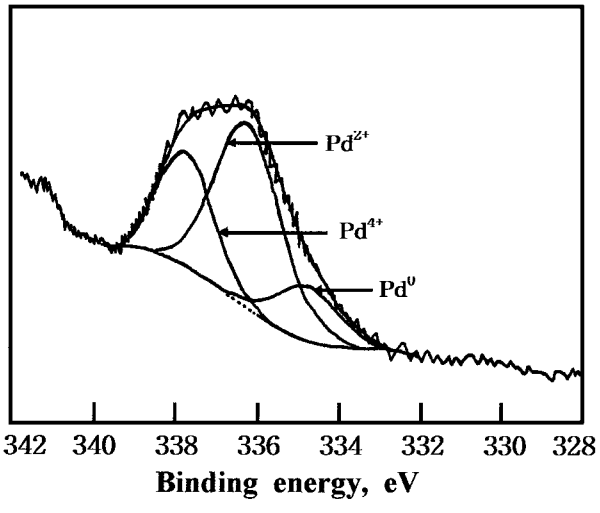

Peak	Centre (eV)	FWHM (eV)	Height (%)	Area (%)
Pd^{4+}	337.7	1.56	55	29
Pd^{2+}	336.2	1.92	87	56
Pd^{0}	334.8	1.70	26	15

FIG. 5. Pd 3*d* XPS of SnO_2/Al_2O_3/Pd (0.2 wt%) sintered at 700°C.

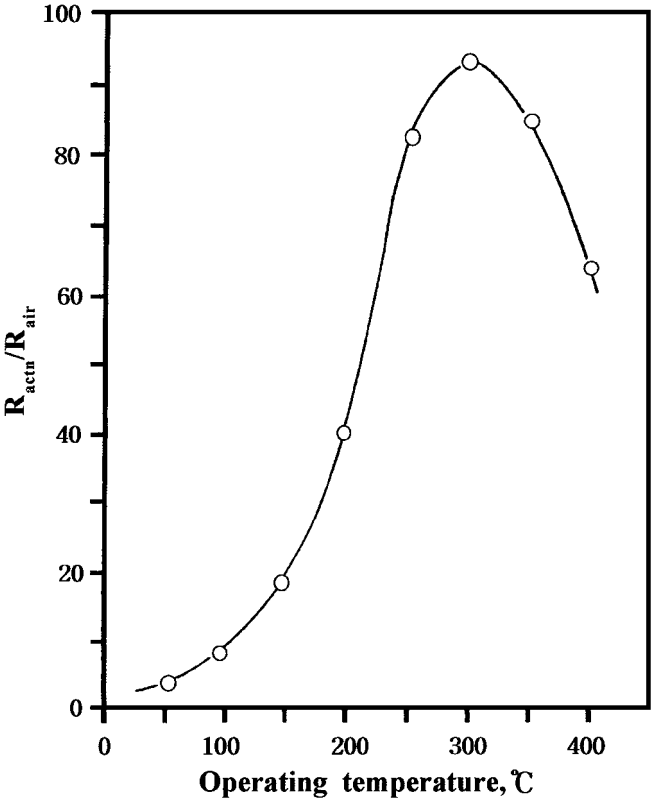

FIG. 6. Sensitivity of the SnO_2/Al_2O_3/Pd (0.2 wt%) thick film device to CH_3CN at various operating temperatures.

The addition of small amounts of additives is known to provide better sensitivity (1, 6, 20). Al_2O_3 was added to improve the stability of the sensor and the adhesion between the sensor and alumina substrate. The addition of Al_2O_3 (10 wt%) increased the sensitivity to CH_3CN. We examined the dependence of the Pd level (0–5.0 wt%) on the sensitivity of the SnO_2/Al_2O_3/Pd sensor when the concentration of CH_3CN was 170 ppm. The devices gave the highest sensitivity at 0.2 wt% Pd, and the optimum operating temperature was 300°C as shown in Fig. 6.

Figure 7 shows IR spectra of oxidation products of CH_3CN on $SnO_2/Al_2O_3/Nb_2O_5$ and $SnO_2/Al_2O_3/Nb_2O_5/SiO_2$ at 300°C for 0.5 h. On $SnO_2/Al_2O_3/Nb_2O_5$, the bands (3723, 3635, 2361, and 667 cm^{-1}) due to CO_2 and the bands (3414, 3334, 964, and 930 cm^{-1}) due to NH_3 were observed similarly to the case of SnO_2 in Fig. 3. However, on a

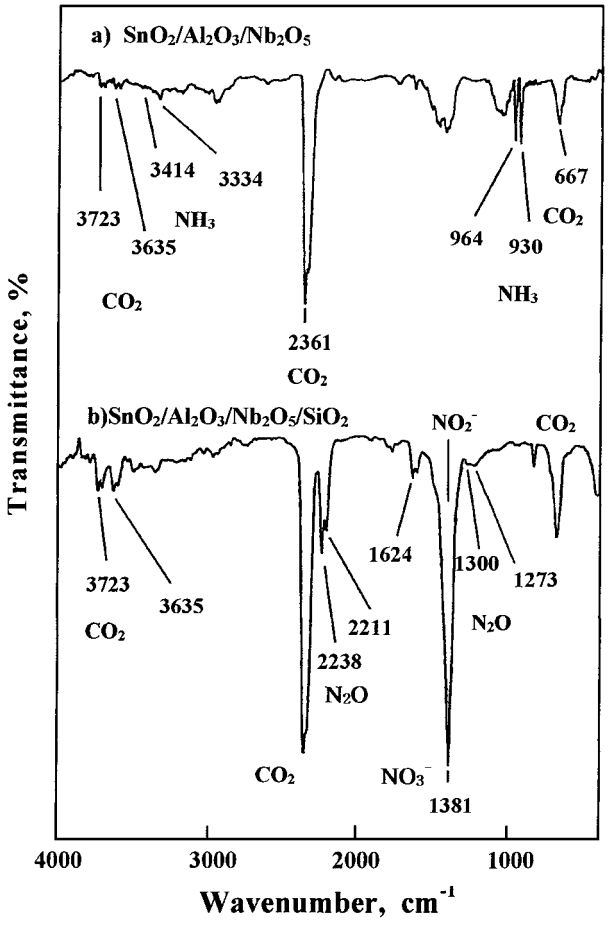

FIG. 7. Infrared spectra after oxidation reaction of CH_3CN on (a) $SnO_2/Al_2O_3/Nb_2O_5$ and (b) $SnO_2/Al_2O_3/Nb_2O_5/SiO_2$ at 300°C for 0.5 h.

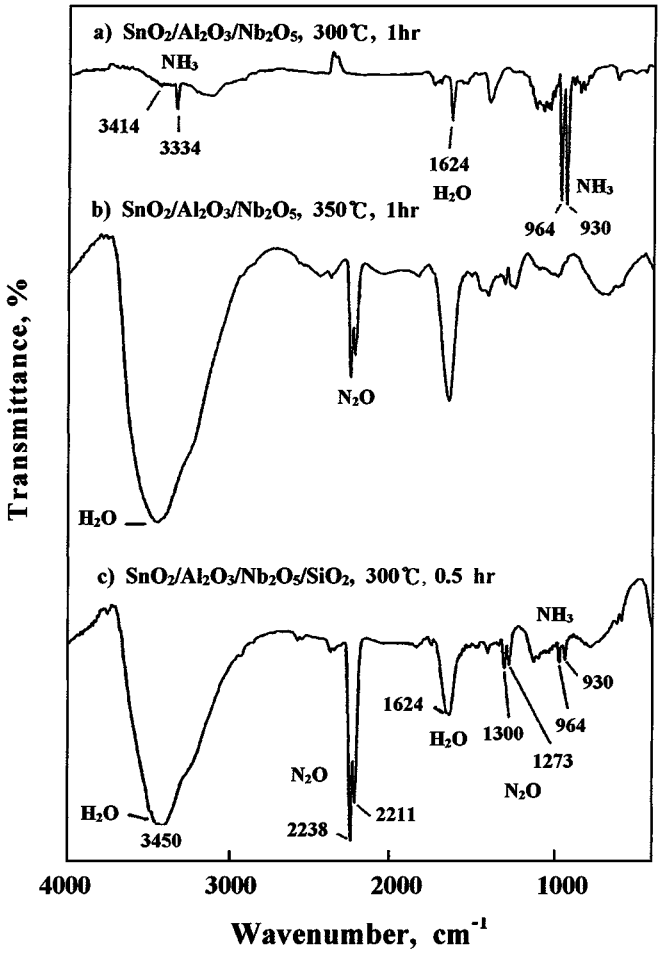

FIG. 8. Infrared spectra after an oxidation reaction of NH_3 on (a, b) $SnO_2/Al_2O_3/Nb_2O_5$ and (c) $SnO_2/Al_2O_3/Nb_2O_5/SiO_2$.

$SnO_2/Al_2O_3/Nb_2O_5/SiO_2$ thick film, N_2O bands instead of NH_3 bands appeared at 2238, 2211, and 1300 cm^{-1} (16). Also, the bands due to the formation of nitrate or nitrite ions were observed at 1381 and 1358 cm^{-1} (16). N_2O also seems to form by the oxidation of NH_3 produced by Eq. [1] according to Eq. [2]. Also, for the IR absorption bands due to nitrate and nitrite groups, the following reaction is assumed to occur (21):

$$2NO_2 + H_2O = HNO_3 + HNO_2. \qquad [3]$$

Oxidation of CH_3CN on a $SnO_2/Al_2O_3/Nb_2O_5$ thick film produced NH_3, as shown in Fig. 7. NH_3 oxidation was carried out in a gas cell to examine the behavior of NH_3 produced on the thick film, where the concentrations of NH_3 and air were 20 and 300 Torr, respectively. The results are illustrated in Fig. 8. After reaction of NH_3 on $SnO_2/Al_2O_3/Nb_2O_5$ at 300°C for 1 h, other products except NH_3 were not detected, while at 350°C the bands of H_2O (3450 and 1624 cm^{-1}) and N_2O (2238 and 2211 cm^{-1}, doublet, and 1300 and 1273 cm^{-1}, doublet) appeared. These results indicate that NH_3 is oxidized by Eq. [2] and the reaction occurs to a greater extent at 350°C than at 300°C. On the other hand, oxidation of NH_3 on $SnO_2/Al_2O_3/Nb_2O_5/SiO_2$ proceeded very easily, even at 300°C, as shown in Fig. 8c. Considering that the operating temperature of the sensor is 300°C, it is expected that the addition of SiO_2 has a significant effect on the characteristics and sensing selectivity of a $SnO_2/Al_2O_3/Nb_2O_5$ sensor.

Specific surface areas of some samples are listed in Table 2. The surface area of $SnO_2/Al_2O_3/Nb_2O_5/SiO_2$ is remarkably large compared to those of the other samples. It

TABLE 2

Specific Surface Areas of Some Samples

Sample	Surface area (m^2/g)
SnO_2	5.0
$SnO_2/Al_2O_3/Pd$	10.5
$SnO_2/Al_2O_3/Nb_2O_5$	22.0
$SnO_2/Al_2O_3/Nb_2O_5/SiO_2$	84.6

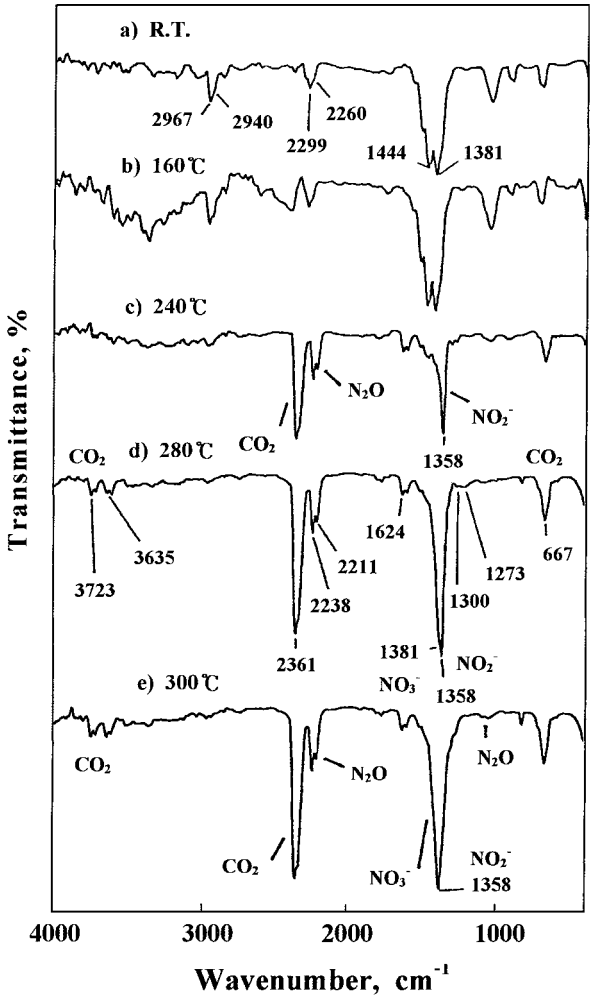

FIG. 9. Infrared spectra after an oxidation reaction of CH_3CN on $SnO_2/Al_2O_3/Nb_2O_5/SiO_2$ at various temperatures for 0.5 h.

seems likely that the surface area also influences the sensing characteristics of the sensor.

Figure 9 shows infrared spectra of gases obtained by oxidation of CH_3CN on $SnO_2/Al_2O_3/Nb_2O_5/SiO_2$ at various temperatures for 0.5 h, where the concentrations of CH_3CN and air are 20 and 300 Torr, respectively. From room temperature to 160°C, no bands except for CH_3CN were observed, indicating that oxidation of CH_3CN did not occur. At 240°C, bands due to CO_2 (2361 cm^{-1}), N_2O (2238 and 2211 cm^{-1}), HNO_3 (1381 cm^{-1}), and HNO_2 (1358 cm^{-1}) appeared and their intensities increased with reaction temperature as shown in Fig. 9. It is known that NH_3, CO_2, and H_2O increase the electric conductivity of a sensor, while N_2O, HNO_3, and HNO_2 decrease the conductivity (13). In view of Figs. 7 and 9, the products formed by oxidation of CH_3CN at 300°C on the $SnO_2/Al_2O_3/Nb_2O_5$ thick film were mainly CO_2, H_2O, and NH_3, while on the $SnO_2/Al_2O_3/Nb_2O_5/SiO_2$ thick film products such as CO_2, H_2O, N_2O, HNO_3, and HNO_3 were observed. Namely, the catalytic activity and selectivity of the above two thick films for the oxidation of CH_3CN are very different. These results explain why $SnO_2/Al_2O_3/Nb_2O_5/SiO_2$ thick film devices show high selectivity and negative sensitivity to CH_3CN. It is clear that the SiO_2 component plays a great role in determining the detection limit of the sensor.

We examined the dependence of the Nb_2O_5 level (0.2–2.0 wt%) on the sensitivity of the $SnO_2/Al_2O_3/Nb_2O_5/SiO_2$ sensor, when the concentration of CH_3CN was 17 ppm and the operating temperature was 300°C. The $SnO_2/Al_2O_3/Nb_2O_5/SiO_2$ devices showed the negative sensitivity by increasing the resistance to CH_3CN, while the $SnO_2/Al_2O_3/Nb_2O_5$ devices without SiO_2 exhibited the positive sensitivity to CH_3CN. As shown in Fig. 10, the devices gave the highest sensitivity at 1.0 wt% Nb_2O_5, showing the increased resistance 22–35 times higher than that in fresh air.

The sensing characteristics of the $SnO_2/Al_2O_3/Nb_2O_5/SiO_2$ device are illustrated as a function of CH_3CN concentration at various operating temperatures in Fig. 11. The sensitivity increased with increasing concentration of CH_3CN and the optimum operating temperature was 300°C. It seems likely that the formation of large amounts

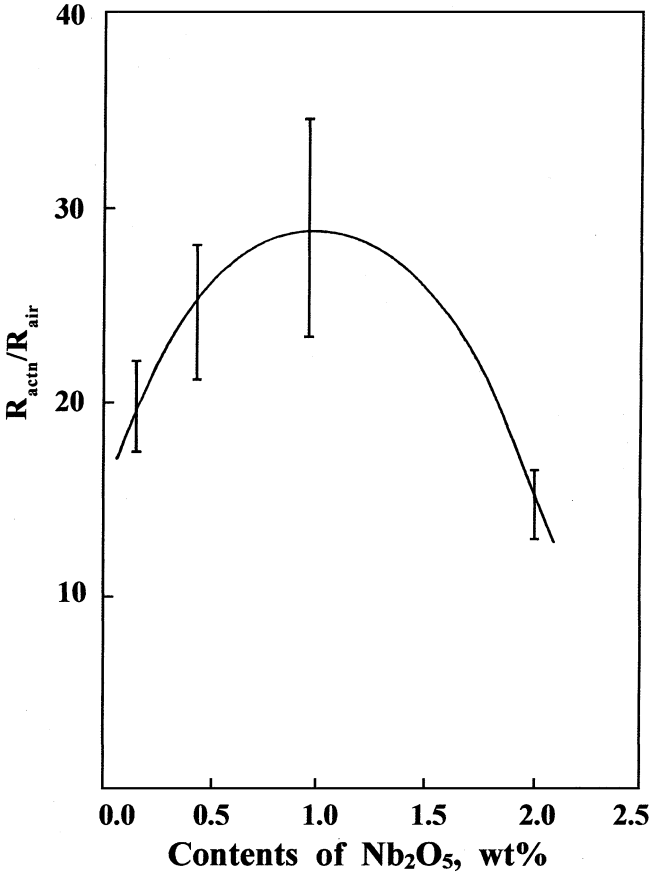

FIG. 10. Sensitivity of the $SnO_2/Al_2O_3/Nb_2O_5/SiO_2$ thick film device to CH_3CN as a function of Nb_2O_5 content at 300°C.

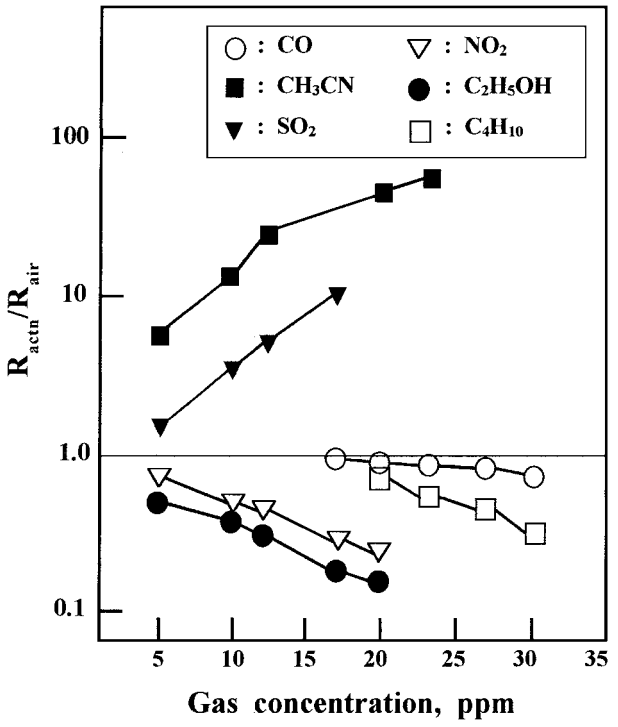

FIG. 11. Sensitivity of the $SnO_2/Al_2O_3/Nb_2O_5/SiO_2$ thick film device to CH_3CN at various operating temperatures.

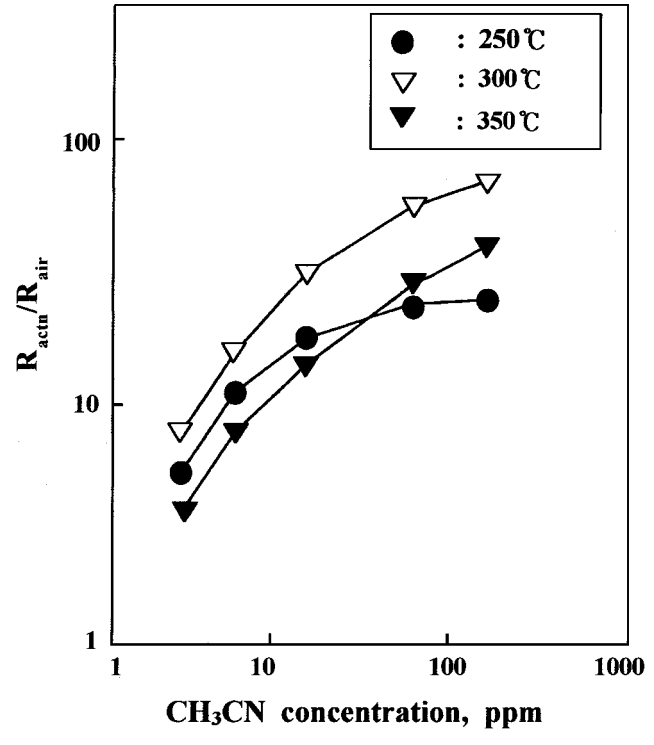

FIG. 12. Resistance characteristics of the $SnO_2/Al_2O_3/Nb_2O_5/SiO_2$ thick film device to various gases at 300°C.

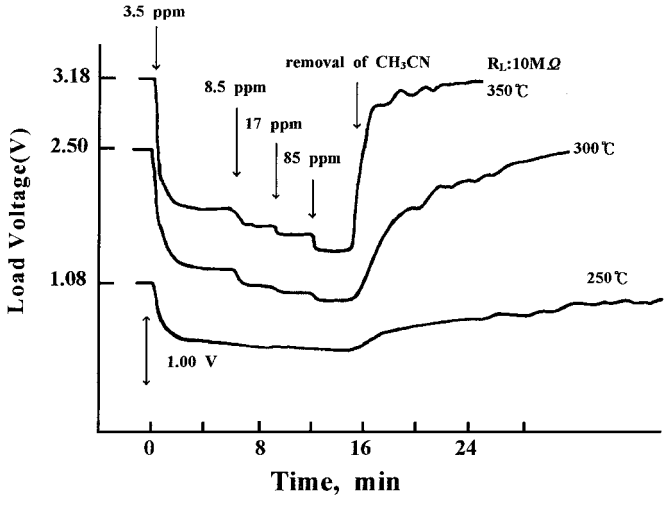

FIG. 13. Transient responses of the $SnO_2/Al_2O_3/Nb_2O_5/SiO_2$ thick film device to CH_3CN at different operating temperatures.

of nitrogen compounds such as N_2O, HNO_3, and HNO_2, which decrease the electric conductivity (13), as shown in Fig. 9, is responsible for the decreased sensitivity at 350°C.

Figure 12 shows sensing characteristics of the $SnO_2/Al_2O_3/Nb_2O_5/SiO_2$ device to various gases at the operating temperature of 300°C. The device exhibited the positive characteristic, resistance decrease, upon exposure to CO, NO_2, C_4H_{10}, and C_2H_5OH, while the device exhibited a negative characteristic upon exposure to CH_3CN and SO_2. These results are in good agreement with the fact that, as shown in Fig. 7, $SnO_2/Al_2O_3/Nb_2O_5/SiO_2$ produces N_2O, HNO_3, and HNO_2, which decrease the electric conductivity of the sensor (13). Therefore, the gas sensor shows high sensitivity and selectivity to CH_3CN among various gases without SO_2. However, since the gas sensor also shows sensitivity to SO_2, as shown in Fig. 12, it is necessary for us to not use the device under the circumstances containing both CH_3CN and SO_2.

Figure 13 shows the transient response characteristics of the $SnO_2/Al_2O_3/Nb_2O_5/SiO_2$ sensor to CH_3CN. The sensor was very sensitive to low gas concentration and the gas sensitivity tended to saturate in the range of high concentration (100 ppm). Also, the sensor showed excellent recovery characteristics as the operating temperature increased. These results indicate that the response characteristics and sensitivity depend on the operating temperature. At 300°C, the response and recovery times are 3 s and 10 min, respectively.

CONCLUSIONS

The SnO_2-based thick film devices for the detection of CH_3CN were fabricated by the screen printing and dipping methods. For the $SnO_2/Al_2O_3/Pd$ thick film, metallic Pd played a great role as a co-catalyst for the oxidation

of CH_3CN. Also, the high surface area of $SnO_2/Al_2O_3/Nb_2O_5/SiO_2$ influenced the sensing characteristics of the sensor. The oxidation products of CH_3CN on a $SnO_2/Al_2O_3/Nb_2O_5/SiO_2$ thick film were CO_2, H_2O, N_2O, HNO_3, and HNO_2. The device exhibited the positive characteristic, resistance decrease, upon exposure to CO, NO_2, C_4H_{10}, and C_2H_5OH, while the device exhibited a negative characteristic upon exposure to CH_3CN and SO_2. The oxidizing agents, such as N_2O, HNO_3, and HNO_2, formed by oxidation of CH_3CN played an important role in determining sensitivity and selectivity to CH_3CN. The response time and the optimum operating temperature were 3 s and 300°C, respectively.

REFERENCES

1. McAleer, J. F., Mosely, P. T., Norris, J. O. W., Williams, D. E., and Tofield, B. C., *J. Chem. Soc. Faraday Trans. 1* **84**, 441 (1988).
2. Seiyama, T., Kato, A., Fujiishi, K., and Nagatanui, M., *Anal. Chem.* **34**, 1502 (1962).
3. Lee, D. D., Sohn, B. K., and Ma, D. S., *Sens. Actuators* **12**, 441 (1987).
4. Torvela, H., Rompainen, P., and Loppävuori, S., *Sens. Actuators* **14**, 19 (1988).
5. Egashira, M., Yoshida, M., and Kawasumi, S., *Sens. Actuators* **9**, 147 (1986).
6. Yamazoe, N., Kurokawa, Y., and Seiyama, T., *Sens. Actuators* **4**, 283 (1983).
7. McAleer, J. F., Moseley, P. T., Norris, J. O. W., Williams, D. E., and Tofield, B. C., *J. Chem. Soc. Faraday Trans. 1* **84**, 441 (1988).
8. Torvela, H., Romppainen, P., and Leppäuori, S., *Sens. Actuators B* **4**, 479 (1991).
9. Fryberger, T. B., and Semancik, S., *Sens. Actuators B* **2**, 305 (1990).
10. Klober, J., Ludwig, M., and Schneider, H. A., *Sens. Actuators B* **3**, 69 (1991).
11. Katsuki, A., and Fukui, K., *Sens. Actuators B* **52**, 30 (1998).
12. Nitta, M., and Haradome, M., *J. Electron. Master* **8**, 571 (1979).
13. Park, H. D., Cho, S. G., Sohn, J. R., and Lee, D. D., *J. Korean Sensor Soc.* **2**, 17 (1993).
14. Sohn, J. R., Cho, S. G., Pae, Y. I., and Hayashi, S., *J. Catal.* **159**, 170 (1996).
15. Knoezinger, H., and Krietenbrink, H., *J. Chem. Soc. Faraday Trans. 1* **71**, 2421 (1975).
16. Nakamoto, K., "Infrared and Raman Spectra of Inorganic and Coordination Compounds." Wiley Interscience, New York, 1978.
17. Schlögl, R., Loose, G., Wesemann, M., and Baiker, A., *J. Catal.* **137**, 139 (1992).
18. Ribeiro, F. H., Chow, M., and Dalla Betta, R. A., *J. Catal.* **146**, 537 (1994).
19. Matsushima, S., Teraoka, Y., Miura, N., and Yamazoe, N., *Jpn. J. Appl. Phys.* **27**, 1798 (1988).
20. Wada, K., and Eqashira, M., *Sens Actuators B* **53**, 147 (1998).
21. Foster, D. S., and Lesline, S. E., "Encyclopedia of Industrial Chemical Analysis." Wiley Interscience, New York, 1978.